Bulletin of the Seismological Society of America, Vol. 78, No. 6, pp. 1885–1906, December 1988

THE JULY 1986 OCEANSIDE (M_L = 5.3) EARTHQUAKE SEQUENCE IN THE CONTINENTAL BORDERLAND, SOUTHERN CALIFORNIA

BY EGILL HAUKSSON AND LUCILE M. JONES

ABSTRACT

An earthquake of M_L = 5.3 occurred at 32°58.7′N, 117°51.5′W southwest of Oceanside in San Diego County at 13:47 13 July 1986 (UT). This main shock was followed by an extensive aftershock sequence, with 55 events of $M_L \geqq 3.0$ during July 1986. The epicenters of the main shock and aftershocks are located at the northern end of the San Diego Trough-Bahia Soledad fault zone (SDT-BS) where it changes strike from northwest to a more westerly direction through a left offset or a bend in the fault. The northwest-striking SDT-BS is one of three strike-slip fault systems that constitute the offshore Agua Blanca fault system. The spatial distribution of the aftershocks indicates a unilateral 7- to 9-km long rupture to the east-southeast away from the epicenter of the main shock. The focal mechanism of the main shock also has an east-southeast striking and south-dipping plane with mostly reverse movement on it. Focal mechanisms of the $M_L \geqq 3.0$ aftershocks show both reverse and strike-slip movement. The reverse focal mechanisms indicate that this sequence may have occurred on a thrust fault that provides for a left stepping offset or a bend in the San Diego Trough fault as movement is transferred to the west along the Santa Cruz-Catalina Island escarpment. Some of the aftershocks that are located to the southeast of the main shock and have strike-slip focal mechanisms suggest activation of the northwest-trending San Diego Trough fault. A stress inversion of the focal mechanism data shows that the maximum principal stress determined from the focal mechanisms of the main shock and 22 aftershocks that occurred within 36 hours of the main shock has an azimuth of S30°W plunging 18°. The maximum principal stress determined from 30 aftershocks that occurred from 15 July to 2 October 1986 has an azimuth of S20°W, plunging 18°. The ϕ-values (the measure of the relative sizes of the principal stresses) are approximately 0.07 and 0.1, respectively, indicating that the intermediate and minimum principal stress are of similar magnitude. The results of the stress inversion, and the focal mechanisms that showed reverse faulting, suggest that the Inner Continental Borderland offshore from Oceanside is not currently a pure-strike-slip tectonic regime but rather a strike-slip mixed with reverse faulting regime. When the 52 aftershock focal mechanisms are divided into four groups and the stress inversion is repeated, the change in stress can be described as a progressive counter-clockwise rotation of 14° of the orientation of the maximum principal stress to a more southerly direction, with the greatest change in stress orientation observed shortly after the main shock. The abundance of aftershocks may be related to the large temporal variation in stress orientation that, in turn, may have resulted from the small stress drop of the main shock.

INTRODUCTION

The 1986 Oceanside earthquake sequence is located 50 to 60 km to the southwest offshore from Oceanside in San Diego county (Figure 1). This sequence does not lend itself easily to detailed analysis because all seismograph stations are located farther away than 50 km. However, because of the abundance of large ($M_L \geqq 3.0$) aftershocks following this earthquake, analysis of this sequence can provide some important insights into understanding aftershock sequences in general, as well as the present day tectonics of the Inner Continental Borderland.

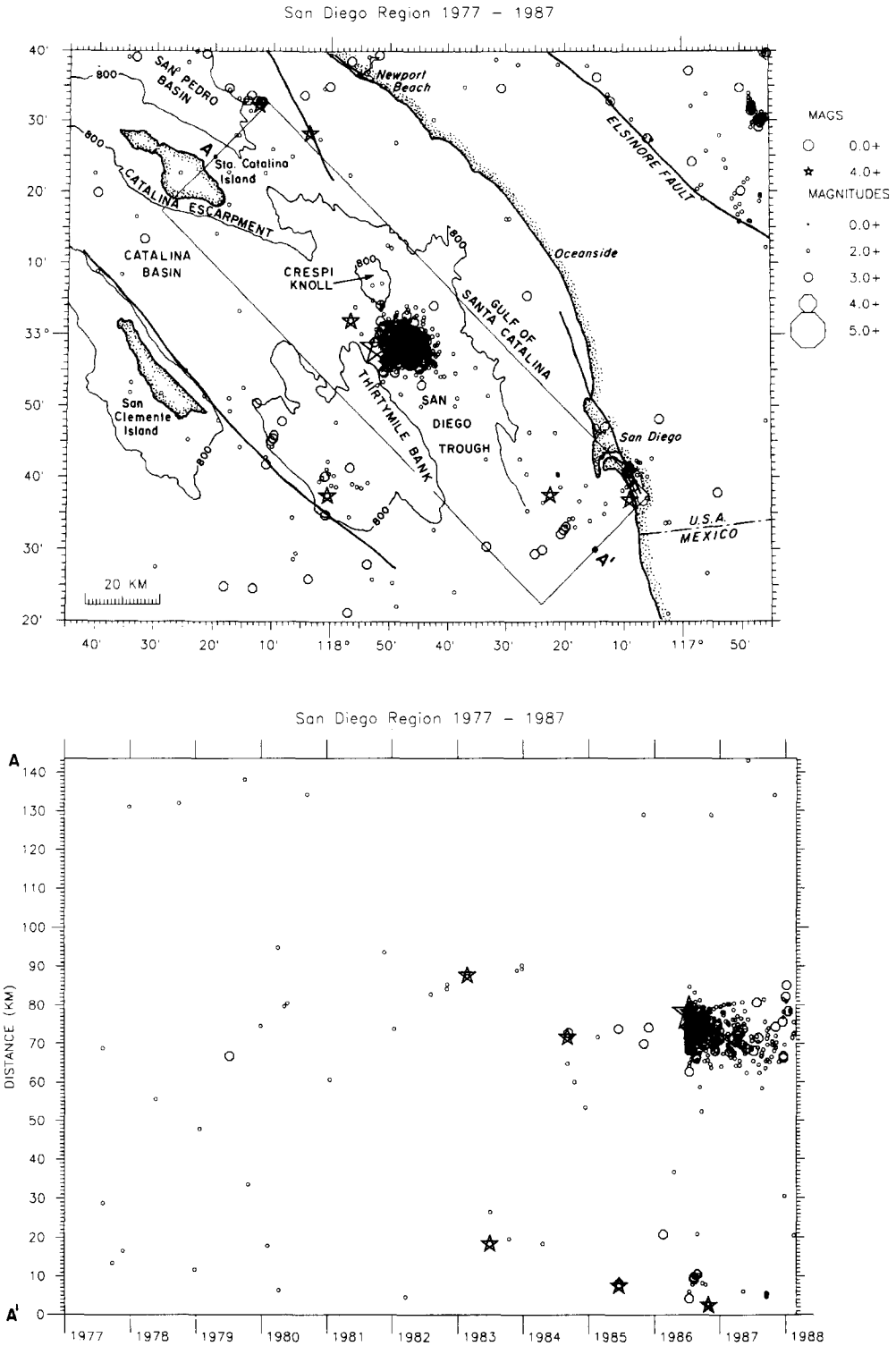

FIG. 1. Seismicity from the CIT/USGS catalog in the Inner Continental Borderland and San Diego Region, southern California. (Top) the seismicity from January 1977 to February 1988. The 800 m bathymetric contour is also shown. Earthquakes located within the box A-A′ are shown in a time-space plot below. Symbol size is scaled with magnitude and events of $M_L \geqq 4.0$ are plotted as stars. (Bottom) time space plot showing level of activity before and after the $M_L = 5.3$ Oceanside main shock.

The Inner Continental Borderland of southern California is dominated by northwest-trending subparallel faults (Legg, 1985). These faults were mapped using acoustic reflection profiling and usually bound topographic highs such as ridges or knolls, or delineate the edges of northwest-southeast elongated basins (Figure 2). The tectonic history of the Continental Borderland extends back to the Jurassic and includes episodes of subduction and transform faulting (Atwater, 1970). The present day tectonics are often described as wrench faulting along the northwest-striking faults; they are attributed to plate boundary deformation between the Pacific and North American plates (Howell and Vedder, 1981).

The Oceanside main shock had a reverse focal mechanism and occurred on an east-southeast striking fault. Such geologic structures have previously been interpreted to be secondary tectonic features associated with the major northwest striking wrench faults (Clarke *et al.*, 1985). The large magnitude of the Oceanside main shock and the abundance of aftershocks however, suggest that these east-trending compressive features are also primary structures, which along with the northwest-striking faults, respond to a stress state with a maximum compressive stress axis trending north-northeast.

The major offshore faults located to the west of Oceanside and San Diego are: 1) the Newport-Inglewood Rose Canyon fault zone straddling the coast line; 2) the Coronado bank fault zone located 20 to 30 km offshore; 3) the San Diego Trough fault located 50 to 60 km offshore; and 4) the San Clemente fault zone 80 km offshore just east of San Clemente Island (Figure 2; Legg, 1985). The first three fault zones converge approximately 100 km south of the international border to form the Agua Blanca fault zone. The San Clemente fault zone continues with a southeast trend offshore from Baja California (Legg, 1985). Because it is difficult, at best, to infer geologic slip rates for offshore faults, it is not possible to tell which fault accommodates the most slip. Most of these northwest-trending faults are well-defined south of 33°N latitude, but as they approach 33°N latitude they step left, and are only shown as dashed lines on the fault map farther to the north (Figure 2; Legg, 1985). The southern boundary of the Santa Catalina Island topographic high, called the Santa Cruz-Catalina Island escarpment, crosses these faults around 33°N latitude trending east-southeast. The tectonic significance of the escarpment is poorly understood. It appears to have a profound influence on the offshore faults, although the escarpment itself does not appear to be associated with significant background seismicity (Figure 1; Legg, 1980). This observation is consistent with the Oceanside earthquake sequence, which appears to provide for a left step or a bend in the San Diego Trough fault rather than being a part of a major east-southeast striking reverse fault that could be associated with the escarpment.

The seismicity (1933 to 1978) of the Inner Continental Borderland is summarized by Legg (1980). He found broad spatial clusters of seismicity that appear to coincide with the major northwest-trending fault zones. His focal mechanisms showed mostly strike-slip and normal faulting but were in most cases not as well-constrained as the focal mechanisms derived in this study. He did not report any focal mechanisms in the immediate vicinity of the Oceanside sequence. He also pointed out that large earthquakes similar to the 1986 Oceanside sequence, with a large number of aftershocks, appear to be a rare occurrence in the Inner Continental Borderland to the west and south of San Diego.

In Figure 1 the seismicity preceding the 1986 Oceanside sequence by 8.5 years and the following 1.5 years of seismicity are shown in both a map view and a space time plot. The 1986 Oceanside sequence was part of the general increase in seismic activity over the whole southern Inner Continental Borderland which began in

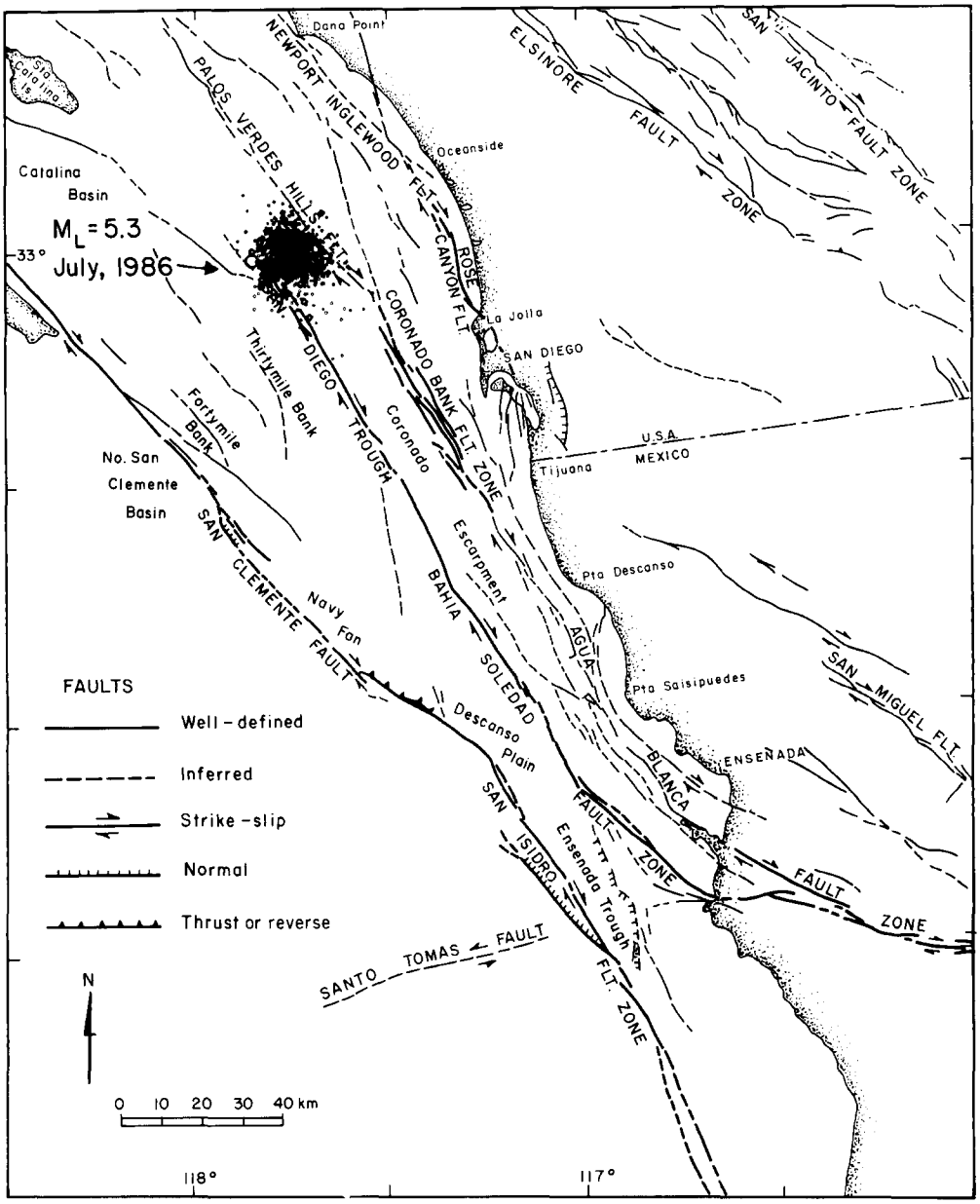

FIG. 2. The 1986 Oceanside ($M_L = 5.3$) main shock-aftershock sequence was associated with the San Diego Trough-Bahia Soledad fault zone. Late Cenozoic offshore faults are from Legg (1985).

1984. Only one $M_L \geqq 4$ earthquake was recorded in the San Diego offshore region between 1932 and 1984, but four $M_L \geqq 4$ events were recorded in the two years preceding the Oceanside earthquake. All $M_L \geqq 3$ earthquakes that occurred during these 2 years were located at one of three sites, the future epicenter of the Oceanside earthquake, a knot in the San Clemente Island fault south of Oceanside, and near the city of San Diego (Figure 1). During the 18 months following 13 July 1986 the most prominent feature on the seismicity map was the Oceanside sequence.

DATA AND TECHNIQUES

The 1986 Oceanside sequence presents some unique problems in obtaining high quality hypocenters and single-event focal mechanisms, because the nearest seis-

mograph station is located 50 to 60 km away, and the maximum azimuthal gap between stations is 170° to 190° (Figure 3). In addition, because most of the earthquakes apparently occurred at a shallow depth (less than 15 km), focal depths and mechanisms will be dependent on the crustal velocity model.

The crustal velocity structure of the Inner Continental Borderland falls halfway between regular continental and oceanic velocity structures with a depth to moho of 22 to 26 km (Corbett, 1984). This thin crust alone suggests that seismicity should be shallow and should occur at depths of less than approximately 15 km. In the case of the 1981 Santa Barbara Island earthquake, the University of Southern California seismograph station on Santa Barbara Island was located at an epicentral distance of 15 to 20 km, and provided some depth control. Corbett (1984) found focal depths for that sequence ranging from 8 to 15 km depth. The focal depths presented here for the Oceanside sequence are similar to the focal depths of the better constrained Santa Barbara Island sequence located 120 km to the northwest.

The velocity model used in this study is based on a model determined by Corbett (1984) for the Inner Continental Borderland using arrival-time data from a large quarry blast, which was detonated on the southeastern end of Santa Catalina Island (Figure 3; Given and Koesterer, 1983). To obtain joint hypocenter locations for the mainshock and aftershocks, the VELEST program (Roecker and Ellsworth, 1978) was used to invert for hypocentral parameters of 53 events, a velocity model, and a set of station delays. A small gradient of increasing velocity with depth was added to Corbett's model to stabilize the focal depths (Figure 4). The arrival times of the Catalina blast were also included to stabilize the VELEST inversion. The velocity model was strongly damped in the VELEST inversion, with station delays

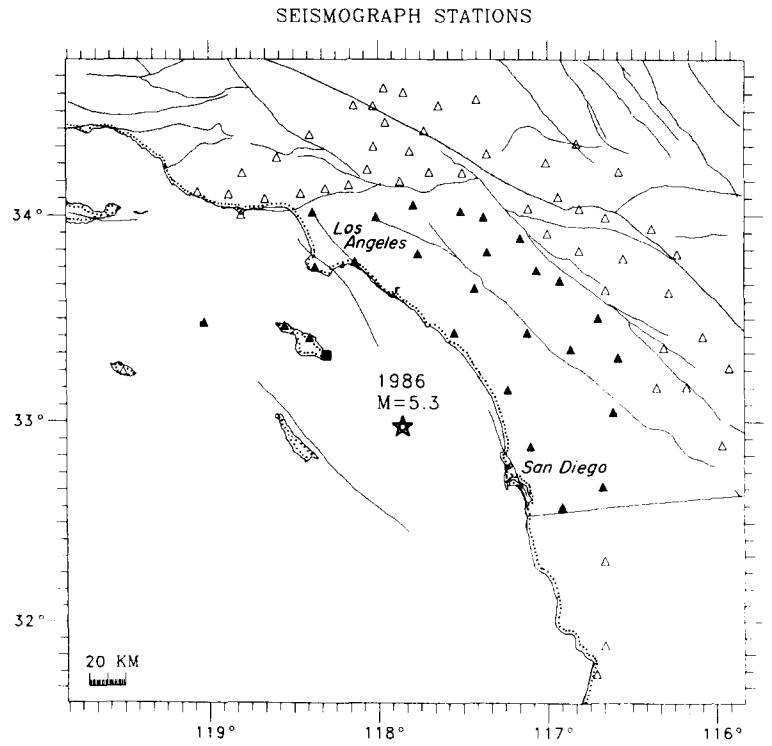

FIG. 3. A map of seismograph stations used to relocate the hypocenters (filled triangles) and determine focal mechanisms (open and filled triangles). The location of the main shock is indicated with a star and the location of the Santa Catalina Island quarry blast is indicated with a solid square.

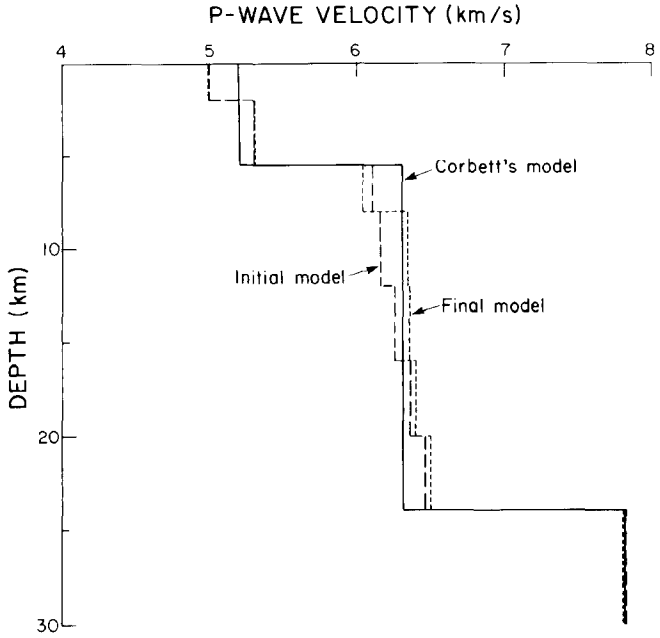

FIG. 4. The crustal P-wave velocity models: the Corbett (1984) model and the initial and final models from the VELEST inversion.

somewhat more damped than the hypocentral parameters. P and S arrival-time data from CIT/USGS and USC seismic network stations located within an epicentral distance of 130 km were included in the inversion (Figure 3). If data from stations at greater distances were included, the inversion became unstable because refracted rays traveling along a single deep refractor in the model start dominating the data set. The final velocity model and corresponding station delays were used with the location algorithm, HYPOINVERSE (Klein, 1985) to relocate the main shock and its aftershocks.

Numerous VELEST inversions done with this data set show that if the velocity structure has lower velocities the earthquake depths increase and vice versa. The final depths, however, appeared to be independent of the chosen starting depth. When the Santa Catalina Island quarry blast was located using the new velocity model and set of stations delays, the calculated location is 1 km south-southeast of the true location. When Corbett's initial model is used, the calculated location of the blast is 2 km south of the true location. The crustal velocity model used in this study also provides a reasonable depth distribution, with a limited number of hypocenters having negative depths or depths greater than 12 km. Because of the inherent limitations in the available data set, the velocity model is not well resolved in the inversion and should be regarded as an average model subject to many trade-offs. Error bars therefore are not included in Figure 4 because these would not reflect accurately the uncertainty in the velocity model.

Single-event focal mechanisms were determined for the main shock and 52 aftershocks of $M_L \geqq 2.9$ which occurred from 13 July to 2 October 1985 (Figure 5 and Table 1). An attempt was made to include all aftershocks of $M_L \geqq 3.0$ in July and all aftershocks of $M_L \geqq 3.4$ that occurred during August, September, and October 1986. Focal mechanisms for several events, however, could not be determined because the first P-wave arrivals were either obscured by the coda of the main shock or they were preceded by immediate foreshocks. To include first motion polarities

from CICESE, Ensenada, Baja California, Mexico, data from stations located within an epicentral distance of 180 km were also included in the focal mechanisms. The three stations located in Baja California, Mexico provide necessary azimuthal coverage to the southeast. All of the digital seismograms were rechecked to ensure consistent picking of first motion polarities and to include all stations within an epicentral range of 180 km. The grid searching algorithm by Reasenberg and Oppenheimer (1985) was used to determine the nodal planes. In cases where the algorithm provided multiple solutions, requiring the nodal planes to be located close to stations with small amplitude or nodal P arrivals was the criteria for selecting a preferred solution. Also, as in the case of the main shock, if a nodal plane coincides with a large amplitude direct P-wave arrival at a nearby station, that mechanism was considered unacceptable.

Several important assumptions have been made to determine the focal depths and mechanisms, which are also tied together through the velocity model. If both the velocity model and therefore the focal depths are incorrect, it can be difficult to fit two orthogonal planes to the distribution of first motion polarities. For instance, the Corbett model was found to give focal mechanisms with fewer inconsistent first motions than other models such as the average southern California model. Hence the distribution of first motions provides some constraints on the velocity model.

The 53 focal mechanisms (Table 1) were used to invert for the orientation of the principal stress axes and a measure of their relative magnitude (ϕ), with a technique developed by Michael (1984). The inversion technique assumes that the direction of the shear stress (i.e., direction of tangential traction) on the fault plane is parallel to the observed slip direction on that plane determined from a focal mechanism. The ϕ-value is defined as $\phi = (S_2 - S_3)/(S_1 - S_3)$ where S_1, S_2, and S_3 are the maximum, intermediate, and minimum principal compressive stresses, respectively. Initial plotting of the focal mechanisms and their respective epicenters indicated that the aftershock activity during the first 36 hours clustered along an east-southeast trend while subsequent activity clustered along a southwest to northeast trend. The focal mechanism data thus were divided into two groups, one consisting of 23 mechanisms of events that occurred during the first 36 hours and the second consisting of 30 mechanisms of events that occurred from 15 July to 2 October 1986.

To determine the orientations of the stress axes and associated 95 per cent confidence limits, it is necessary to choose one plane from each focal mechanism as being the actual fault plane. For the reverse faulting mechanisms the south-dipping planes were chosen. The northwest-trending planes, subparallel to the offshore faults, were chosen for the strike-slip focal mechanisms. In a few cases of north-south-striking reverse mechanisms, the planes dipping west were chosen. These planes are listed in Table 1. This choice of planes also gave consistently lower average misfit angles in the stress inversion than the corresponding set of auxiliary planes.

RESULTS

The 1986 Oceanside earthquake occurred 50 km southwest of the City of Oceanside in San Diego county at 13:47 13 July 1986 (U.T.) and was followed by a large aftershock sequence (Figure 6). The main shock of $M_L = 5.3$ was followed by four aftershocks of $M_L \geqq 4.0$ and 95 aftershocks of $M_L \geqq 3.0$ from 13 July to 30 April 1987. This abundance of aftershocks makes this sequence the largest aftershock sequence recorded (1932 to 1987) for a $M_L < 5.5$ main shock in southern California. The aftershock sequence also had a high b-value of 1.32 ± 0.07.

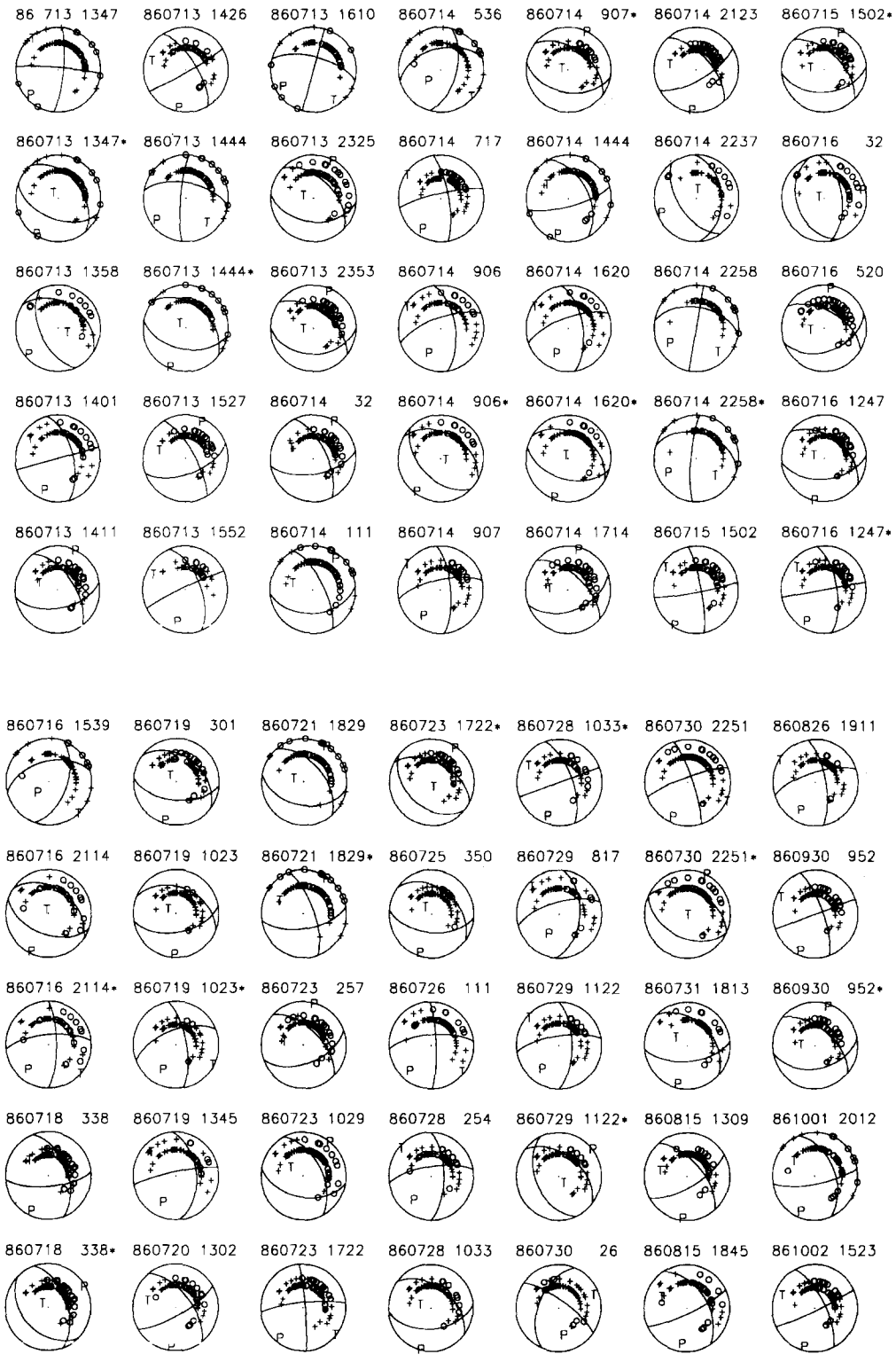

FIG. 5. Lower-hemisphere single-event focal mechanisms for the Oceanside main shock and 52 aftershocks. Plus symbol indicates compressional first motion polarities while open circles indicate dilatational first motion polarities. Each mechanism is labeled with date and time of occurrence. Multiple solutions for each event are flagged by a star. Nodal planes were determined using the Reasenberg and Oppenheimer (1985) grid searching algorithms.

TABLE 1

HYPOCENTERS AND FOCAL MECHANISMS OF THE 1986 OCEANSIDE MAIN SHOCK AFTERSHOCK SEQUENCE

No	Date	Time		Location				Depth km	Mag	Focal Mechanism		
				Latitude		Longitude				Ddir	Dip	Rake
1	07/13/86	1347	8.2	32	58.7	117	51.5	8.8	5.3	200.0	50.0	70.0
2	07/13/86	1358	50.4	32	59.4	117	47.1	7.5	3.3	245.0	55.0	110.0
3	07/13/86	1401	32.8	33	0.2	117	50.0	7.3	4.6	75.0	60.0	180.0
4	07/13/86	1411	0.5	32	58.6	117	47.4	4.9	3.7	170.0	55.0	40.0
5	07/13/86	1426	1.3	32	58.7	117	45.6	4.9	3.6	58.2	70.1	174.7
6	07/13/86	1444	41.5	32	58.7	117	46.6	8.1	3.1	190.0	50.0	70.0
7	07/13/86	1527	7.4	32	58.7	117	43.5	2.0	3.3	160.0	60.0	20.0
8	07/13/86	1552	9.2	32	59.2	117	46.4	4.2	3.1	67.9	60.0	−174.2
9	07/13/86	1610	17.8	32	57.4	117	47.1	9.2	3.2	285.0	90.0	155.0
10	07/13/86	2325	13.3	32	59.4	117	44.0	6.2	3.4	185.0	45.0	60.0
11	07/13/86	2353	42.6	32	59.4	117	45.0	2.5	3.6	180.0	40.0	60.0
12	07/14/86	32	46.0	32	59.7	117	47.2	4.8	4.0	170.0	60.0	30.0
13	07/14/86	111	10.3	32	57.9	117	49.2	8.0	3.7	175.0	45.0	30.0
14	07/14/86	536	44.6	32	57.8	117	50.2	8.7	3.4	105.0	60.0	−130.0
15	07/14/86	717	34.7	32	59.6	117	47.3	0.2	3.6	80.0	75.0	−170.0
16	07/14/86	906	47.3	32	57.5	117	47.7	6.5	2.9	81.2	62.0	−157.2
17	07/14/86	907	53.8	32	59.6	117	47.7	4.7	3.6	85.0	70.0	−160.0
18	07/14/86	1444	8.4	32	58.7	117	49.0	8.8	3.7	165.0	75.0	40.0
19	07/14/86	1620	9.6	32	59.3	117	49.6	7.0	3.4	81.2	62.0	−157.2
20	07/14/86	1714	42.8	32	60.0	117	45.1	5.4	3.4	160.0	50.0	40.0
21	07/14/86	2123	9.4	32	58.6	117	44.3	0.5	3.1	150.0	70.0	30.0
22	07/14/86	2237	7.9	33	0.8	117	48.3	7.5	3.0	235.0	55.0	70.0
23	07/14/86	2258	49.8	32	57.2	117	47.7	8.2	3.1	275.0	80.0	130.0
24	07/15/86	1502	45.2	32	58.9	117	43.6	4.7	3.1	79.1	80.0	174.9
25	07/16/86	32	32.8	33	0.2	117	50.1	6.2	3.0	250.0	35.0	80.0
26	07/16/86	520	50.7	33	0.8	117	45.6	3.7	3.2	160.0	45.0	50.0
27	07/16/86	1247	1.1	32	58.3	117	48.3	2.7	3.7	175.0	50.0	60.0
28	07/16/86	1539	17.8	32	58.0	117	50.0	8.2	3.0	110.0	55.0	−130.0
29	07/16/86	2114	2.2	32	58.2	117	48.3	6.7	3.0	90.0	70.0	40.0
30	07/18/86	338	40.4	33	1.8	117	42.8	0.0	3.0	175.0	70.0	40.0
31	07/19/86	301	21.2	33	1.2	117	44.2	4.0	3.0	185.0	55.0	70.0
32	07/19/86	1023	38.6	32	58.2	117	48.3	1.3	3.1	170.0	55.0	70.0
33	07/19/86	1345	26.4	32	57.7	117	48.9	6.8	3.2	85.0	50.0	−170.0
34	07/20/86	1302	23.0	32	57.4	117	45.2	2.9	3.3	150.0	75.0	30.0
35	07/21/86	1829	30.8	33	1.1	117	48.1	8.4	3.8	190.0	45.0	60.0
36	07/23/86	257	58.2	32	59.9	117	47.3	4.4	3.5	160.0	55.0	40.0
37	07/23/86	1029	1.6	33	0.8	117	49.0	6.2	3.4	190.0	50.0	50.0
38	07/23/86	1722	16.5	33	1.4	117	43.8	4.3	3.3	85.0	85.0	−170.0
39	07/25/86	350	7.6	32	58.9	117	48.2	0.1	3.0	185.0	55.0	70.0
40	07/26/86	111	49.5	32	58.0	117	49.2	7.8	3.0	88.4	80.6	−159.7
41	07/28/86	254	45.7	32	57.2	117	48.7	5.0	3.6	90.0	65.0	−160.0
42	07/28/86	1033	9.2	32	58.3	117	48.7	4.5	3.2	175.0	50.0	60.0
43	07/29/86	817	41.4	32	56.7	117	49.7	5.6	4.3	95.0	50.0	−150.0
44	07/29/86	1122	22.4	32	57.4	117	48.9	5.1	3.5	90.0	65.0	−160.0
45	07/30/86	26	29.7	32	57.8	117	48.4	2.2	3.4	35.0	75.0	−140.0
46	07/30/86	2251	13.0	33	0.7	117	46.9	6.6	3.9	205.0	45.0	90.0
47	07/31/86	1813	39.7	32	57.7	117	48.6	7.6	3.3	175.0	60.0	60.0
48	08/15/86	1309	46.9	33	0.7	117	46.9	4.8	3.4	150.0	70.0	30.0
49	08/15/86	1845	16.1	32	56.9	117	47.8	5.6	3.7	155.0	80.0	40.0
50	08/26/86	1911	49.9	32	56.1	117	49.5	5.3	3.5	80.0	70.0	−160.0
51	09/30/86	952	11.2	33	0.5	117	46.6	0.1	3.9	170.0	45.0	50.0
52	10/01/86	2012	18.3	32	58.4	117	50.4	8.5	4.0	170.0	75.0	40.0
53	10/02/86	1523	28.6	33	0.6	117	45.2	0.1	3.4	63.2	70.1	174.7

Latitude in degrees and minutes; longitude in degrees and minutes; local magnitude from CIT/USGS catalog; Ddir = dip direction in degrees; Dip = dip in degrees; and Rake = rake in degrees.

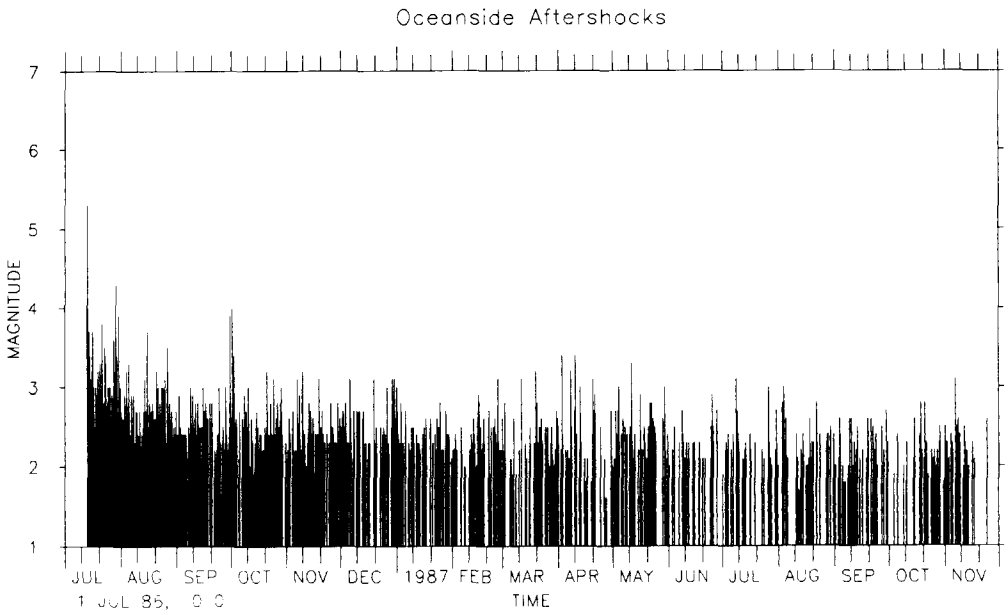

FIG. 6. Magnitude versus time for the Oceanside aftershocks.

Earthquake hypocenters. The main shock epicenter (32°58.7′N and 117°51.5′W) is located at the western edge of the aftershock zone (Figure 7a). The aftershocks that occurred in July 1986 show a scattered distribution to the east and northeast of the main shock with a small gap in the distribution just northeast of the main shock epicenter. The depth distribution of aftershock hypocenters projected on a N20°E striking plane (normal to the nodal planes in the focal mechanisms) is shown in Figure 7b. The focal depths are clearly model dependent because the closest seismograph station is located 50 to 60 km away and the crustal velocity structure is not well known. The depth distribution obtained from HYPOINVERSE using the velocity model and corresponding station delays from VELEST could differ significantly, if a proper network of ocean bottom seismographs was deployed to record some events for depth calibration. The depth distribution determined by HYPOINVERSE is used in this study, because the relative spatial distribution of the epicenters is not strongly dependent on the calculated focal depths. An alternative approach could be to ignore the depths from HYPOINVERSE and assign arbitrary fixed depths of 6 to 10 km to all of the earthquakes. This approach would also be unsatisfactory in that what little information about depth there is in the P and S arrival time data, would be ignored. By using the depths from HYPOINVERSE the implicit assumption is simply that the overall broad features of the depth distribution may be correct but many of the detailed features are probably artifacts.

Because the main shock had a reverse faulting focal mechanism, the epicentral distribution alone in Figure 7a can be used to evaluate which nodal plane was the actual fault plane by assuming that the main shock ruptured from depth up toward the earth's surface. Surface projections of both planes from the focal mechanism are shown in Figure 7a. The scattered epicentral distribution of aftershocks indicates that the south-dipping plane is a more likely rupture surface than the north-dipping plane. A south-dipping plane falls within the distribution of aftershocks. A north-dipping plane, however, would fall outside the distribution of aftershocks, assuming

only that the relative epicentral locations of the main shock and its aftershocks are correct. The diffuse depth distribution of the $M_L \geqq 3.0$ aftershocks in Figure 7b support the interpretation that the south-dipping nodal plane was the actual fault plane.

The distribution of aftershocks that occurred from August 1986 to April 1987 is similar to the distribution reported in July 1986 (Figures 8a and 8b). The scattered distribution becomes more pronounced while the quiescent zone of no aftershocks remains immediately northeast of the main shock epicenter. At this stage the

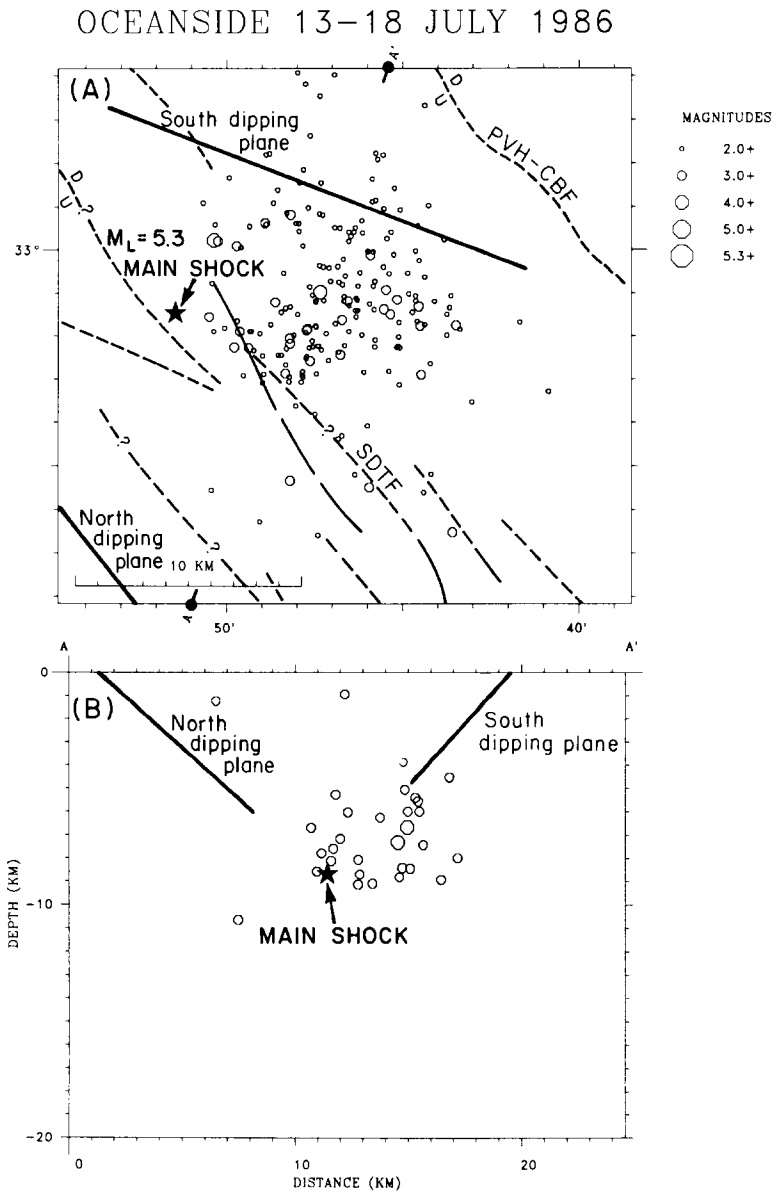

FIG. 7a. The main shock and $M_L \geq 2.0$ aftershocks from 13 July to 18 July 1986 with location and depth errors ERZ $\leqq$ 3.0 km and ERH $\leq$ 3.0 km as determined by HYPOINVERSE. The approximate surface projections of the south-dipping nodal plane and the north-dipping plane from the main shock focal mechanism are also plotted.

FIG. 7b. Depth cross section along the A-A′ in Figure 7a. Only earthquakes of $M_L \geq 3.0$ are included. The nodal planes from the main shock focal mechanism are also shown.

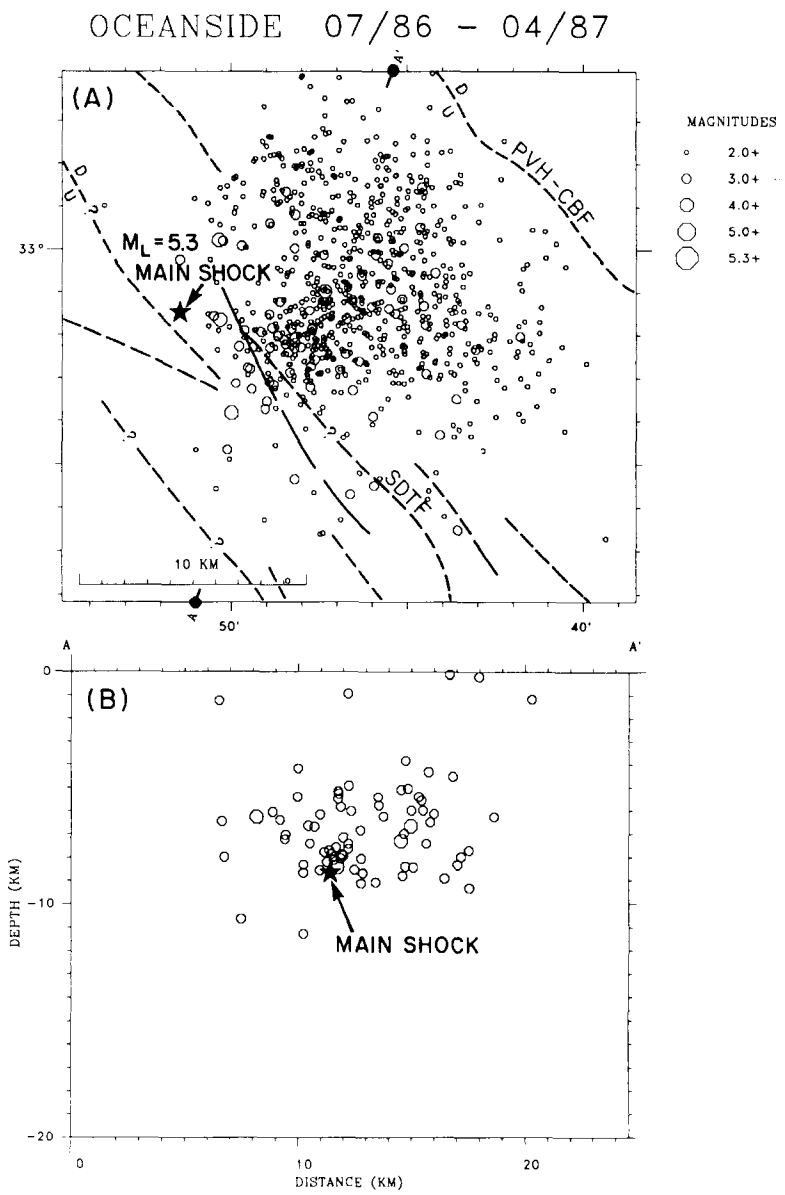

FIG. 8a. The main shock and $M_L \geq 2.0$ aftershocks from July 1986 to April 1987 with location and depth errors of ERZ $\leq$ 3.0 km and ERH $\leq$ 3 km as determined by HYPOINVERSE.

FIG. 8b. Depth cross section along the line A-A′ in Figure 8a. Only earthquakes of $M_L \geq 3.0$ included.

aftershock zone can be viewed as consisting of an east-southeast trend with a more diffuse southwest-northeast trend superimposed. The strongest cluster of activity is located a few kilometers east of main shock epicenter.

To investigate possible relationships between the location of the Oceanside sequence, the bathymetry of the sea floor and offshore faults, all of the recorded hypocenters from July 1986 to April 1987, and offshore faults (from Clarke *et al.*, 1988) are plotted on the topographic map of the ocean floor in Figure 9. The Oceanside sequence is located in the vicinity of a complex junction of many offshore faults. The sequence is located closest to the San Diego Trough fault as it branches out of the San Diego Trough and turns westward. The aftershock zone begins at

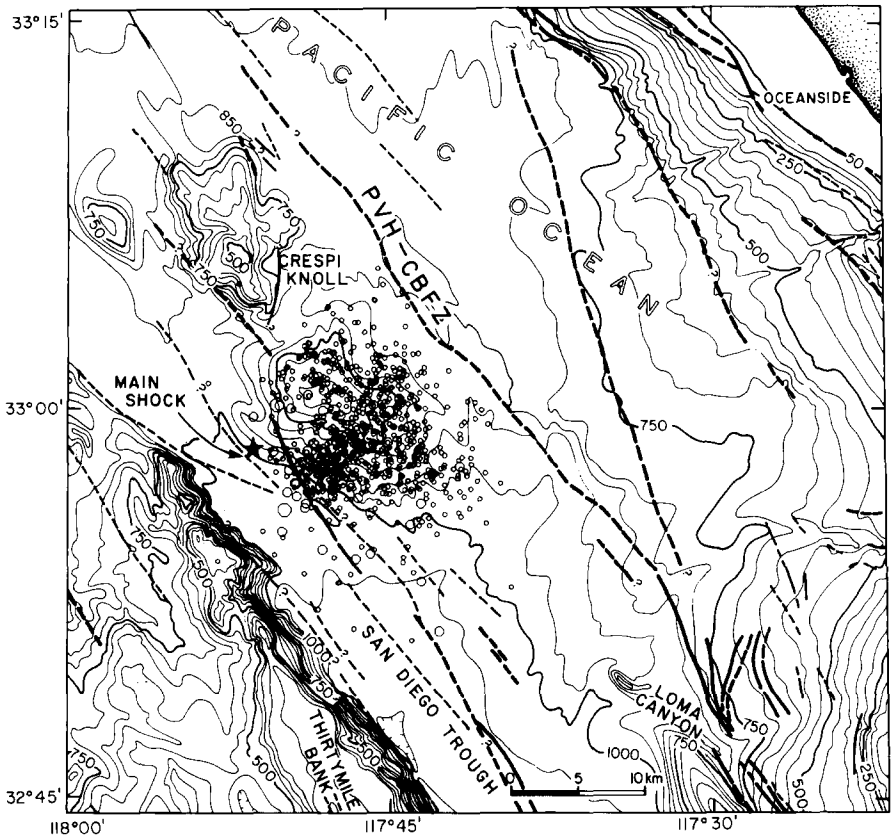

FIG. 9. The main shock (shown as a star) and all aftershocks from July 1986 to April 1987 plotted on a bathymetric map of the study area. Offshore faults are from Clarke *et al.* (1988). PVH-CBFZ-Palos Verdes Hill-Coronado Bank Fault Zone. Faults with known Holocene offsets are plotted as thick lines. Inferred faults are shown as dashed lines.

the main shock in the left step of the San Diego Trough fault (SDTF) and fans out to the east beneath a small knoll located just south of Crespi knoll. Some activity is also observed to the south along the main surface trace of the San Diego Trough fault itself. If the main shock ruptured a south-dipping fault, the surface expression of the fault would be expected between the two knolls. The aftershock zone has a total length of 7 to 9 km and extends 3 to 5 km to the east of the left step in the SDTF toward the Coronado Bank fault zone. A left step or a bend in the Coronado Bank fault is suggested in Figure 9 where the fault forms two branches, one with a northerly strike and a second forming the southwest extension of the Palos Verdes Hill fault. Both of these branches are only inferred (Clarke *et al.*, 1988; Legg, 1985). If the Palos Verdes Hill fault is assumed to be relatively inactive in this region, the Oceanside sequence could also be providing for a left step in the Coronado Bank fault. Such a conclusion, however, is highly speculative at this stage.

Focal mechanisms. The single-event lower-hemisphere focal mechanisms for the main shock and 52 aftershocks are plotted for two time intervals, the first 36 hours following the main shock and 15 July to 2 October 1986 in Figure 10. The two nodal planes of the main shock focal mechanism strike N70°W with a dip of 50° to the south and N40°W with a dip of 40° to the north. The focal mechanism of the main shock and the south-dipping distribution of aftershock hypocenters suggest that the fault ruptured by the main shock is the N70°W striking and south-dipping plane.

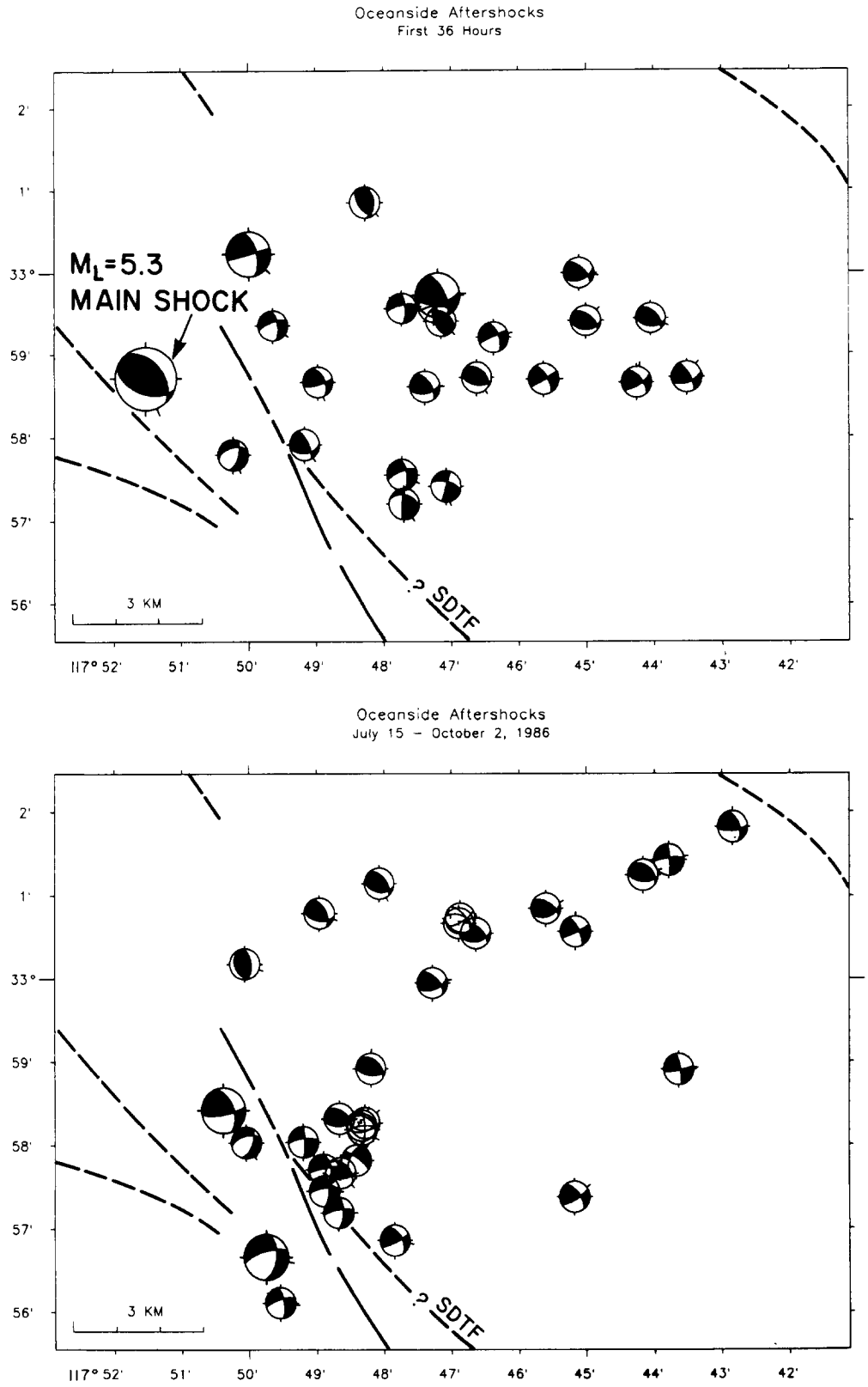

FIG. 10. Single-event lower-hemisphere focal mechanisms for the Oceanside sequence. Shaded areas are compressional quadrants. (Top) the main shock focal mechanism and focal mechanisms of $M_L \geq 3.0$ aftershocks recorded during the first 36 hours following the main shock. (Bottom) The focal mechanisms of the main shock and $M_L \geq 3.0$ aftershocks from 15 July to 2 October 1986.

This observation is also consistent with the knoll above the sequence being uplifted by south over north crustal movement.

The preliminary focal mechanism of the main shock was initially reported as strike-slip on a north-trending plane (Given *et al.*, 1987). Because a strike-slip mechanism requires the north-south nodal plane to be adjacent to the high-amplitude direct P-wave arrivals, the reverse mechanism was preferred for the main shock after visually inspecting the digital seismograms. Pacheco and Nábělek (1988), who analyzed teleseismic data from the main shock, also found a reverse mechanism with a strike of N47 ± 2°W, dip of 48 ± 1°, and rake of 109 ± 1°. Their focal mechanism is very similar to the reverse focal mechanism derived from local data. They also determined a seismic moment of $6.5 \pm 0.7 \times 10^{24}$ dyne-cm ($M_S = 5.8$) with a stress drop of 27 bars. The large difference between the M_L and M_S magnitudes suggests that relatively larger proportion of radiated energy was radiated as long-period waves than short-period waves.

Approximately half of the 52 aftershock focal mechanisms are consistent with reverse faulting similar to that observed for the main shock. The other aftershock focal mechanisms are mostly strike-slip mechanisms that in a few instances have a small component of normal faulting. This variety in the type of focal mechanisms is common for aftershock sequences in southern California (e.g., Jones *et al.*, 1986; Hauksson *et al.*, 1988). Figure 10 also illustrates the temporal development of the aftershock zone for the $M_L \geqq 3.0$ aftershocks. During the first 36 hours following the main shock, the aftershock zone extends as a 2 km wide zone approximately 7 to 9 km to the east (Figure 10). During the subsequent two months the $M_L \geqq 3.0$ aftershocks form two spatial clusters; one is located 2 to 4 km southeast of the main shock, while the second is located 8 to 10 km to the northeast of the main shock (Figure 10). The southeast cluster has mostly strike-slip mechanisms, which suggests that some of these aftershocks may be occurring on the San Diego Trough fault itself. The northeast cluster, however, is not associated with a mapped fault structure. The distribution of large aftershocks and their focal mechanisms thus suggests that the reverse faulting main shock may have activated adjacent segments of northwest-trending strike-slip faults.

The inversion of the whole data set of 53 focal mechanisms yields an average principal stress trending S25°W and plunging 18°. The inversion of the focal mechanism data that was done for the main shock and the first 22 aftershocks yields a principal stress trending S30°W and plunging 18° (Table 2 and Figure 11). The inversion of the subsequent 30 aftershocks yields a principal stress trending S20°W plunging 19°. The ϕ-values (the measure of the relative sizes of the principal stresses) are 0.07 and 0.1 respectively, indicating that the intermediate and minimum principal stresses are of approximately the same magnitude. The absolute size of the change in orientation of the maximum principal stress axis of 10° is approximately half the size of the change that was observed for the larger ($M_L = 6.6$) Coalinga 1983 main shock (Michael, 1987B). The 95 per cent confidence limits for the orientations of the stress axis as determined using bootstrap techniques developed by Michael (1987A), are shown in Figure 11. The probability density function for the rotation determined from 2000 bootstrap results shows that at the 95 per cent confidence level this observed change in stress orientation is significant. The stress inversion requires that one nodal plane is selected from each focal mechanism, as a possible fault plane. To account for possible incorrect choices of planes, the stress inversion was also done assuming that 30 per cent of the planes were picked incorrectly. Although the 95 per cent confidence limits are somewhat

TABLE 2

STRESS INVERSION RESULTS FOR THE 1986 OCEANSIDE EARTHQUAKE SEQUENCE

Window	Events	First days	Mean days	Last days	PHI	β	MAX COMP AZ
	01–53	0.0	40.5	81.0	0.06 ± 0.20	12.7 ± 12.6	−154.7 ± 5.0
	01–23	0.0	0.7	1.5	0.07 ± 0.21	13.4 ± 12.3	−149.5 ± 8.0
	24–53	2.0	39.5	81.0	0.10 ± 0.18	11.2 ± 12.5	−159.4 ± 5.0
A	02–14	0.0	0.3	0.6	0.21 ± 0.18	08.8 ± 10.4	−148.0 ± 7.0
B	15–28	2.0	0.6	1.3	0.16 ± 0.26	17.9 ± 12.0	−153.4 ± 16.0
C	29–41	3.3	5.6	11.2	0.18 ± 0.15	08.9 ± 07.2	−158.5 ± 7.0
D	42–53	14.8	33.1	81.0	0.12 ± 0.14	06.9 ± 05.9	−162.2 ± 6.0

Window = Time windows whose principal stress axes are shown in Figure 12; Events = Events grouped together where numbers of events refer to table 1; First = Start day of time window since the time of main shock; Mean = Mean time of time window; Last = Last day of time window; PHI = The relative stress magnitudes; β = The misfit angle in degrees; COMP AZ = Azimuth of principal stress axis in degrees west of north.

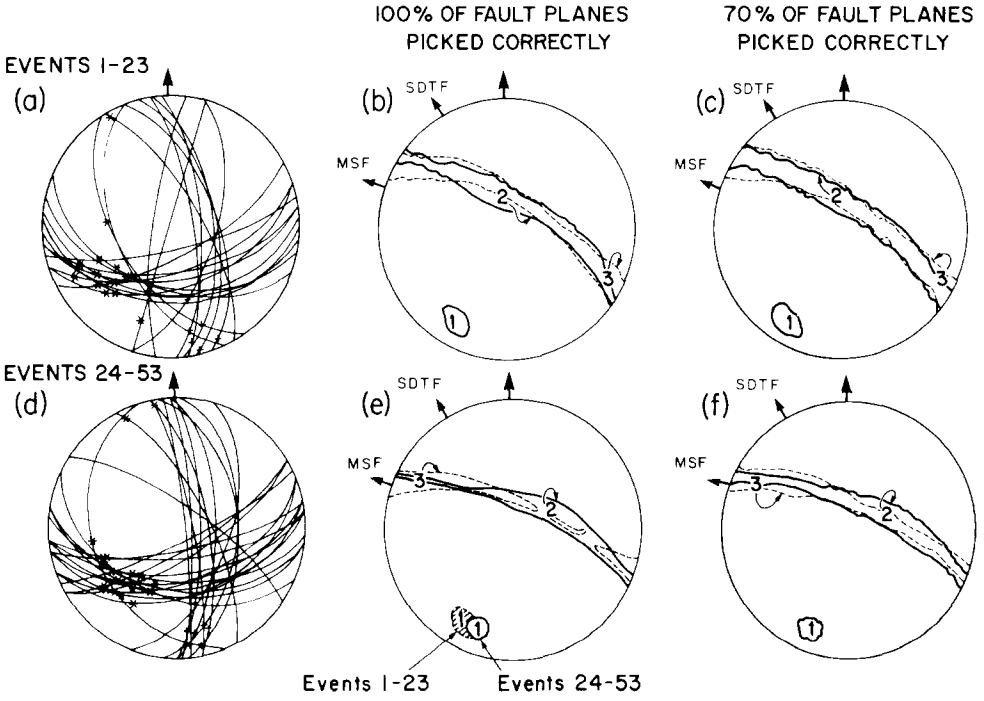

FIG. 11. Data and results of the stress inversion: (a) Lower hemisphere projection of all nodal planes (one from each focal mechanism) from the main shock and 22 aftershocks that occurred during the first 36 hours following the main shock. Location of the slip vector is shown on each nodal plane as a plus symbol (with a normal component) or a star (with a thrust component); (b) The corresponding orientations of the principal stress axes with 95 per cent confidence areas indicated with solid or dashed lines. 1, 2, and 3 are maximum, intermediate, and minimum principal stress axes, respectively. The azimuthal orientations of the San Diego Trough fault (SDTF) and the assumed main shock fault (MSF) are also shown; (c) Same as (b) except 30 per cent of the planes are assumed to be picked incorrectly; (d) Nodal planes from focal mechanisms of 30 aftershocks that occurred from 15 July to 2 October 1986; (e) The correponding orientations of the principal stress axes with 95 per cent confidence areas indicated with solid or dashed lines. For comparsion, the orientation and 95 per cent confidence interval of the compressional axis from the first 23 events is also shown; (f) Same as (e) except 30 per cent of the planes are assumed to be picked incorrectly.

larger than for the case of all planes being assumed correct, the rotation of the maximum principal stress axis is still significant (Figure 11). The average misfit angles listed in Table 2 are also a measure of the quality of the inverse solutions.

The strike of the San Diego Trough fault and the south-dipping plane of the

Oceanside main shock focal mechanism are also shown on the stereographic projection Figure 11. The maximum principal stress axis of the second stress state forms a high angle of 50° to 60° with the San Diego Trough fault but a low angle 30° to 40° with the south-dipping plane of the focal mechanism of the main shock. Hence the south-dipping reverse fault may have experienced higher shear stress than the northwest-trending San Diego Trough fault. The observed change in orientation of the principal stress is also accompanied by a relative increase in strike-slip focal mechanisms as compared to the number of reverse focal mechanisms. However, although the spatial distributions of the two sets of aftershocks are different, they overlap the same region and the change in stress with time is therefore not thought to result from spatial variations. Rather, the variation appears to be temporal. To analyze the decay of the stress anomaly with elapsed time, the data set of 52 aftershock focal mechanisms was divided into four sets of 13 mechanisms each and the stress inversion was repeated (Table 2). The orientations of the principal stress axes for the four time windows are shown in a stereo projection in Figure 12. The results from these inversions show that the orientation of the compressional principal stress decays smoothly with time, indicating that the stress state is

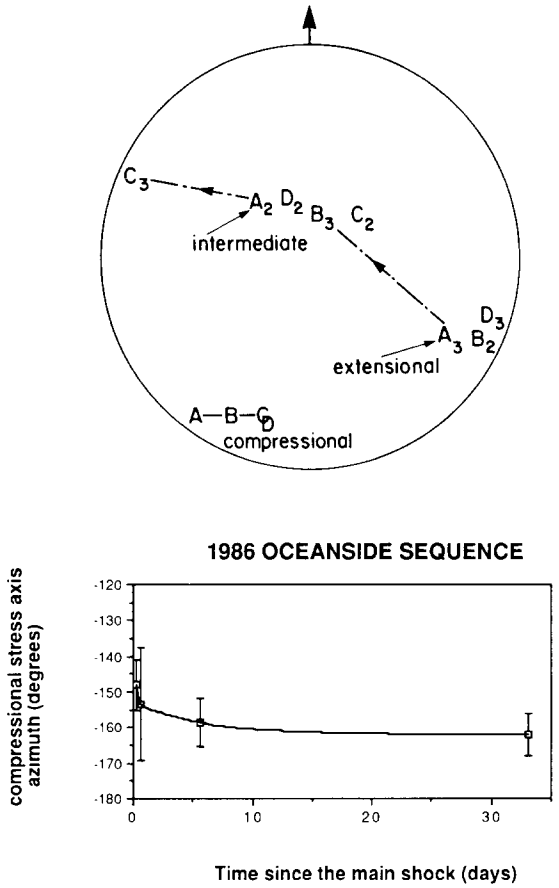

FIG. 12. (Top) Rotation of principal stress axes obtained by dividing the data set into four temporal groups as is shown in Table 2. A–D refers to the group while letters without a subscript refer to maximum axis and with subscripts refer to (3—minimum, 2—intermediate) stress axes. (Bottom) Azimuthal orientation of the maximum principal stress axis in degrees west of north versus time since the main shock. The error bars are 96 per cent confidence limits.

decaying either back to a pre-main shock stress state or to a new stress state that will recover over the interseismic period back to the pre-main shock stress state (Figure 12). Because the minimum and intermediate principal stresses are of similar magnitude, these show large variations with large 95 per cent confidence intervals.

DISCUSSION

Although the Oceanside main shock was a relatively small earthquake and caused little damage, it illustrates that offshore faults are seismogenic and could present significant seismic hazards. The Oceanside sequence also contained several surprises: 1) the main shock showed reverse faulting on an east-southeast striking plane that dips to the south; 2) the main shock was followed by a large aftershock sequence, and 3) a significant change in the orientation of the compressional principal stress axis can be identified following the main shock.

The Inner Continental Borderland is cross cut by three major northwest striking fault systems (Legg, 1980, 1985). The 1986 Oceanside sequence occurred within one of these systems, the San Diego Trough-Bahia Soledad fault zone. Geologic interpretation of seismic reflection and sonar data shows that this system mostly accommodates strike-slip motion, although locally, at fault bends or other discontinuities, transpressive or transtensive features have been mapped (Legg, 1985). The Oceanside sequence ruptured a south-dipping reverse fault, which may be a transpressive feature at a left step in the San Diego Trough fault at the northern end of the San Diego Trough. The transpressive feature is also expressed by an uplifted knoll, located just south of Crespi knoll. Although the location of the Oceanside sequence beneath the knoll may be coincidental, the colocation of the knoll and the Oceanside sequences suggests that some of these knolls may be active tectonic features. The origin of these shield-shaped uplifts, called knolls, in the Continental Borderland is not clearly understood although dredged rocks from their slopes are mostly volcanic in origin (Legg, 1985).

The north-dipping nodal plane in the main shock focal mechanism is not considered to be the actual fault plane, although it strikes parallel to the surface trace of the San Diego Trough fault. If the north-dipping plane was the actual fault plane, the San Diego Trough fault would have to be a reverse fault, which is contrary to the geologic finding of Legg (1985) and Clarke *et al.* (1988). Furthermore, as previously discussed, if the main shock ruptured from depth up to the surface, its relative epicentral location with respect to the aftershock distribution is not consistent with a north-dipping fault plane. Hence the south-dipping nodal plane is preferred as the actual fault plane.

Clarke *et al.* (1985) interpreted the major northwest-striking offshore faults in the Borderland as being wrench faults. Possible folding and en-echelon small faults that may form transpressive or transtensive tectonic features along or adjacent to the major fault trends, were interpreted to be secondary tectonic features resulting from the wrench faulting. This tectonic model of the Continental Borderland implies that the deformation along the Pacific-North America plate boundary extends into the Borderland. Furthermore, it implies that tectonic blocks within the Continental Borderland are colliding with different velocities into the western Transverse Ranges. Because different blocks move with different velocities, regions of local compression and tension would be expected adjacent to one another along the southern margin of the western Transverse Ranges. Such stress patterns have not been documented (Hauksson, 1987).

The state of stress within the Inner Continental Borderland as determined from

the 30 aftershocks, occurring from 15 July to 2 October 1986, shows a N20°E trending maximum principal stress axis with the intermediate and minimum principal stresses of similar magnitude. Such a stress state facilitates mostly strike-slip faulting along northwest-striking faults with some reverse faulting along east-west-striking faults. This stress state is consistent with Legg's (1985) mapping of the San Diego Trough fault, where he identifies mostly strike-slip offsets. At the northern end of the Trough, the fault encounters the Santa Catalina topgraphic high and the strike of the fault trends to the west along the escarpment of this topographic high. This change in strike of the fault thus coincides with a change in style of deformation from strike-slip to reverse faulting.

The 1986 Oceanside earthquake sequence ruptured an east-southwest-striking reverse fault which suggests a model of tectonic deformation within the Continental Borderland that differs from the wrench faulting model. The Continental Borderland, like most of southern California west of the San Andreas fault, is in a stress state with a horizontal maximum principal stress trending north-northeast. Hence if the strike-slip movements on the northwest-trending faults are assumed to be small, the faulting caused by the tectonic stress field will cause reverse faulting on east to south-southeast-striking faults and strike-slip faulting on northwest- to north-striking faults. A mixture of reverse and strike-slip faulting may also occur on faults with orientations between north and east. In this scenario, most of the tectonic blocks of the Continental Borderland would be moving to the northwest with similar velocities. In addition, they would cause a fairly continuous front of tectonic deformation along the southern margin of the western Transverse Ranges. A recently revised estimate of Pacific-North America relative plate motion shows the discrepancy between geologic and geodetic estimates is only 5 mm/yr, instead of previous estimates of 15 mm/yr. Their estimate supports the idea that the strike-slip motion on northwest-striking offshore faults may be small (DeMets *et al.*, 1987).

A rotation in the orientation of the maximum principal stress similar to that documented here for the Oceanside sequence was also observed in the aftershocks following the 1983 Coalinga (Michael, 1987B) and 1986 North Palm Springs (Michael and Jones, 1986) earthquakes but not following the 1987 Whittier Narrows earthquake (Hauksson *et al.*, 1988). As Michael (1987B) pointed out, a rotation in principal stress orientation is also a change in stress magnitude although the rotation and change in magnitude are not necessarily directly proportional. He suggested that after the stress drop in the main shock, recovery occurs and the state of stress returns from its new anomalous state to a pre-main shock state over a time period of months. This is shown schematically with the stress recovery model in Figure 13. The final stress state should be the same as the pre-main shock stress state. At Coalinga too few earthquakes preceded the main shock to determine the state of stress before the main shock but Michael infers it to be similar to his final state from geologic evidence.

This pattern of stress recovery (Figure 13) is similar in form to the strains measured near major plate boundaries during the postseismic period (Thatcher, 1984). Thatcher noted the quick recovery of a fraction of the strain drop as compensating for "coseismic overshooting". He attributed this short-term partial recovery (months to years) to aseismic slip or viscoelastic response (postseismic slip) of the asthenosphere. The strain would recover completely over the much larger interseismic period. Time-delayed response was also necessary to explain the concentration of strain near the San Andreas fault in the interseismic period

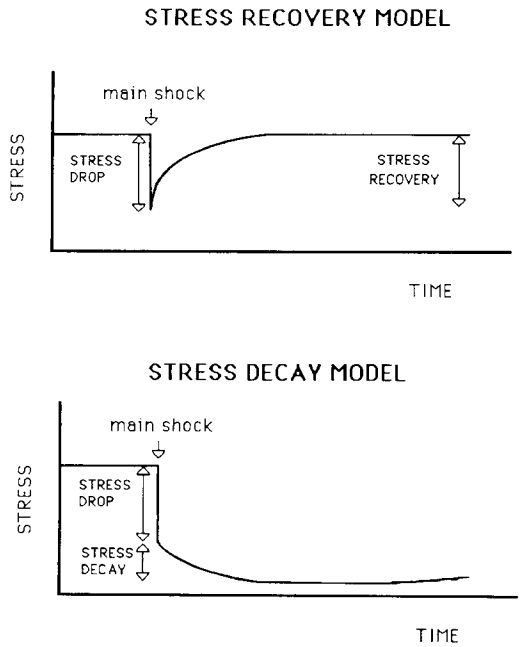

FIG. 13. A schematic diagram showing how stress changes with time in a constant stress recovery model and a stress decay model. The coseismic stress drop is followed by stress decay or recovery that consists of changes in the orientations of the principal stress axes. In the recovery model the stress decay makes the stress return to the long-term geologic stress. Alternatively, in the decay model the stress decay is a continuation of the main shock stress drop and only during the interseismic period does the stress begin to return to the long-term geologic stress.

(Thatcher, 1983). The occurrence and temporal decay of aftershocks has also been attributed to aseismic slip loading patches (Wesson, 1987) or viscoelastic deformation (Sibson, 1983).

Although recorded strain at a point shows a partial recovery after a large earthquake, this does not require the stress to recover (move in the opposite sense from the initial stress drop). At a point near or on the fault, the strain will drop during the main shock. After the main shock, its aftershocks, aseismic slip, or viscoelastic creep cause further movement, and the point that was initially relieved can quickly be partially reloaded. However, the average stress, averaged over the whole fault plane, will decrease as illustrated in the stress decay model in Figure 13. It seems reasonable to consider the average post-main shock stress change to be in the same sense as the coseismic stress drop because aftershocks in general have the same focal mechanisms as their main shock. In addition, the events with significant stress rotations (Oceanside and Coalinga) exhibit relatively low stress drops and large numbers of aftershocks. By contrast, Whittier Narrows had no recognizable stress rotation, a very high stress drop, and very few aftershocks (Michael, 1989). These data can be explained by the stress decay model in Figure 13.

If the absolute strength of rock does not vary greatly, a high stress drop event can be considered to be better coupled than a low stress drop event, so that a greater percentage of the fault plane actually slips in the event. Thus, for a high stress drop event, only a small area would need to slip after the main shock, leading to few aftershocks and a small stress decay. By contrast, a poorly-coupled event would have a small coseismic average stress drop and require considerable post-main shock

slip leading both to more aftershocks and larger stress rotations. This observation is compatible with the correlation found by Tajima and Kanamori (1985) between greater expansion of aftershock zones with time after poorly-coupled main shocks. Of course, coupling of the main shock is only one of many factors, such as regional stress state and fault segmentation, that could influence the stress decay and the abundance of aftershocks. Hence, the small stress drop of the main shock, the large stress decay, and the abundance of aftershocks in the Oceanside sequence suggest that the main shock was poorly coupled, and was followed by significant postseismic slip.

Conclusions

The 1986 Oceanside main shock had a reverse focal mechanism and probably ruptured the east-southeast-striking and south-dipping plane. The sequence was associated with the San Diego Trough-Bahia Soledad fault zone. The aftershock zone extends approximately 7 to 9 km from west to east-southeast. The focal mechanisms of the aftershocks show reverse and strike-slip faulting. The abundance of aftershocks may be related to the significant change in the state of stress that was observed following the main shock. The Oceanside sequence may have occurred on a thrust fault that provides for a left offset or a bend in the San Diego Trough fault as it curves toward the west around the Santa Cruz-Catalina Island escarpment. The results of the stress inversion of the focal mechanisms data and the reverse faulting observed in the main shock suggest that the Inner Continental Borderland is not a pure strike-slip tectonic regime but is rather a mixture of a strike-slip and reverse faulting regime. Hence tectonic crustal deformation is accommodated with strike-slip movement along approximately north-striking faults and reverse movement along approximately west-striking faults.

Acknowledgments

We thank J. McRaney, J. Eaton, A. Michael, and C. Nicholson for critically reviewing the manuscript. Dr. José Frez C. provided information about the polarity of stations located in Baja California, Mexico. A. Michael made his computer programs available for the stress inversion. J. Pacheco and J. Nábělek provided a preprint of their paper. This research was supported by USGS Grant 14-08-0001-G1328 and USGS Contract 14-08-0001-A0264. The manuscript by typed by Desser Moton.

References

Atwater, T. (1970). Implications of plate tectonics for the cenozoic tectonic evolution of western North America, *Geol. Soc. Am. Bull.*, **81**, 3513–3536.

Clarke, S. H. Jr., H. G. Greene, and M. P. Kennedy (1985). Identifying potentially active faults and unstable slopes offshore, in *Evaluating Earthquake Hazards in the Los Angeles Region: An Earth-Science Perspective*, J. I. Ziony, Editor, *U.S.G.S. Prof. Paper 1360*, 347–374.

Clarke, S. H., H. G. Green, M. P. Kennedy, and J. G. Vedder (1988). California Continental Margin Geologic Map Series, *Geology of the Inner-Southern California Continental Margin*, H. G. Greene and M. P. Kennedy, Editors, California Division of Mines and Geology, Sacramento.

Corbett, E. J. (1984). Seismicity and crustal structure studies of southern California: tectonic implications from improved earthquake locations, *Ph.D. Thesis*, California Institute of Technology, Pasadena.

DeMets, C., R. G. Gordon, S. Stein, and D. F. Argus (1987). A revised estimate of Pacific-North America motion and implications for western North America plate boundary zone tectonics, *Geophys. Res. Lett.*, **14**, 911–914.

Given, D. D. and C. L. Koesterer (1983). Station arrival data for a quarry blast on Santa Catalina Island, California, *U.S. Geol. Surv., Open-File Rept. 83-462.*

Given, D. D., L. M. Jones, L. K. Hutton, and S. Hartzell (1987). The Southern California Network Bulletin July through December, 1986, *U.S. Geol. Surv., Open-File Rept. 87-488*, Pasadena, California.

Hauksson, E. (1987). Seismotectonics of the Newport-Inglewood fault zone in the Los Angeles basin, southern California, *Bull. Seism. Soc. Am.*, **77**, 539–561.

Hauksson, E., L. M. Jones, T. L. Davis, L. K. Hutton, G. Brady, P. A. Reasenberg, A. J. Michael, R. F. Yerkes, P. Williams, G. Reagor, C. W. Stover, A. L. Bent, A. K. Shakal, E. Etheridge, R. L. Porcella, C. G. Bufe, M. J. S. Johnston, and E. Cranswick, (1988). The 1987 Whittier Narrows earthquake in the Los Angeles metropolitan area, California, *Science*, **239**, 1409–1412.

Howell, D. G. and J. Vedder (1981). Structural implications of stratigraphic discontinuities across the Southern California Borderland, in *The Geotectonic Development of California (Rubey Volume I)*, W. G. Ernst, Editor, Prentice-Hall, Englewood Cliffs, New Jersey, 535–558.

Jones, L. M., L. K. Hutton, D. D. Given, and C. R. Allen (1986). The North Palm Springs, California, earthquake sequence of July 1986, *Bull. Seism. Soc. Am.*, **76**, 1830–1837.

Klein, F. W. (1985). User's guide to HYPOINVERSE, a program for VAX and PC350 computers to solve for earthquake locations, *U.S. Geol. Surv., Open-File Rept. 85-515*, Menlo Park, California.

Legg, M. R. (1980). Seismicity and tectonics of the Inner Continental Borderland of southern California and northern Baja California, Mexico, *M.S. Thesis*, University of California at San Diego.

Legg, M. R. (1985). Geologic structure and tectonics of the inner Continental Borderland offshore northern Baja California, Mexico, *Ph.D. Thesis*, University of California at Santa Barbara.

Michael, A. J. (1984). Determination of stress from slip data: faults and folds. *J. Geophys. Res.*, **89**, 11517–11526.

Michael, A. J. (1987A). Use of focal mechanisms to determine stress: a control study *J. Geophys. Res.*, **92**, 357–368.

Michael, A. J. (1987B). Stress rotation during the Coalinga of shock sequence *J. Geophys. Res.* **92**, 7963–7979.

Michael, A. J. (1989). Stress analysis of the Whittier Narrows, California, aftershock sequence, submitted to *J. Geophys. Res.*

Michael, A. J. and L. M. Jones (1986). Stress fluctuations due to the North Palm Springs earthquake, *Trans. Am. Geophys. U.*, **67**, p. 1090.

Pacheco, J. and J. Nábělek (1988). Source mechanisms of three moderate southern California earthquakes of July 1986, *Bull. Seism. Soc. Am.*, **78**, 0000–0000.

Reasenberg, P. and D. Oppenheimer (1985). FPFIT, FPPLOT and FPPAGE: Fortran computer programs for calculating and displaying earthquake fault-plane solutions, *U.S. Geol. Surv., Open-File Rept. 85-739.*

Roecker, S. and Ellsworth, W. L. (1978). VELEST, Fortran Program, U.S. Geol. Surv., Menlo Park, California.

Sibson, R. H. (1983). Continental fault structure and the shallow earthquake source, *J. Geol. Soc. London*, **140**, 741–767.

Tajima, F. and H. Kanamori (1985). Global survey of aftershock area expansion patterns, *Phys. Earth Planet. Interiors*, **40**, 77–134.

Thatcher, W. (1983). Nonlinear strain buildup and the earthquake cycle on the San Andreas fault, *J. Geophys. Res.*, **88**, 5893–5902.

Thatcher, W. (1984). The earthquake deformation cycle, recurrence, and the time-predictable model, *J. Geophys. Res.*, **89**, 5674–5680.

Wesson, R. L. (1987). Modelling aftershock migration and afterslip of the San Juan Bautista, California, earthquake of October 3, 1972, *Tectonophysics*, **144**, 215–219.

UNIVERSITY OF SOUTHERN CALIFORNIA
DEPARTMENT OF GEOLOGICAL SCIENCES
LOS ANGELES, CALIFORNIA 90089-0740
(E.H.)

UNITED STATES GEOLOGICAL SURVEY
525 SOUTH WILSON AVENUE
PASADENA, CALIFORNIA 91106
(L.M.J.)

Manuscript received 25 April 1988